PASJ: Publ. Astron. Soc. Japan , 1–??,

Plasma parameters in a post-eruptive arcade observed with CORONAS-F/SPIRIT, Yohkoh/SXT, SOHO/EIT, and in microwaves

Victor V. Grechnev, Arkadii M. Uralov, Vasily G. Zandanov, George V. Rudenko
Institute of Solar-Terrestrial Physics, Irkutsk, Russia
grechnev@iszf.irk.ru
Valery N. Borovik, Irina Y. Grigorieva
Main Astronomical Observatory, St. Petersburg (Pulkovo), Russia
borovik@MK4099.spb.edu
Vladimir A. Slemzin, Sergey A. Bogachev, Sergei V. Kuzin, Igor' A. Zhitnik, Andrey A. Pertsov
P.N.Lebedev Physical Institute, Moscow, Russia
kuzin@sci.lebedev.edu
Kiyoto Shibasaki
Nobeyama Radio Observatory, Japan
shibasaki@nro.nao.ac.jp
and
Moisey A. Livshits
IZMIRAN, Troitsk, Russia
livshits@izmiran.troitsk.ru

(Received 2000 December 31; accepted 2001 January 1)

Abstract

The SPectroheliographIc X-Ray Imaging Telescope (SPIRIT) complex aboard the CORONAS-F spacecraft launched in August 2001 sometimes observes in the high-temperature MgXII 8.42 Å line (temperature sensitivity range 5–20 MK with a maximum at about 9 MK) relatively large, bright features existing for many hours high in the corona. This fact suggests the possibility that plasma beta in those features might not be small. We identify such a hot feature, which was observed in the MgXII line on October 22, 2001 above the limb at a height of about 100 Mm, with a high-temperature part of a post-eruptive arcade. Using *Yohkoh*/SXT images, other multi-spectral data, and radio astronomy methods, we estimate plasma parameters in the arcade and reveal the large-scale coronal magnetic field configuration. Several hours after the eruption, the temperature in the arcade is 6–8 MK, and the plasma density is $(5-10)\cdot 10^9$ cm^{-3}. We confirm the results by the accord of the quantities obtained from different observations using different methods and by extrapolation of the photospheric magnetic fields into the corona, from which we have obtained the magnetic field strength of about 7 G at that height. Hence, indeed we deal with $\beta \geq 1$ in the post-eruptive arcade. The high-beta possibility had been already stated in some previous publications, e.g., by Ichimoto, Sakurai, et al. in 1993, but still neither thoroughly investigated, nor even attracted the common attention. We then discuss implications of this fact in terms of the "standard flare model" elaborated by Shibata & Yokoyama to incorporate calculations of the chromospheric evaporation. Another particularity of this event is related to dark features observed with *Yohkoh*/SXT to move downward onto the arcade, first discovered by McKenzie and Hudson. We find those features to represent structures filled in with cold material, if they are not empty. They may also affect the arcade.

Key words: Sun: corona — Sun: X-rays, gamma rays — Sun: UV radiation — Sun: radio radiation — Sun: magnetic fields

1. Introduction

The CORONAS-F space solar observatory (Oraevsky & Sobelman 2002) was launched in August 2001. The CORONAS-F spacecraft operates in an orbit of the Earth and contains several solar telescopes and spectrometers to record thermal and non-thermal emissions.

The **SP**ectrograph**I**c X-**R**ay **I**maging **T**elescope (SPIRIT; Zhitnik et al. 2002) aboard the CORONAS-F contains several extreme-ultraviolet (EUV) and soft X-ray telescopes and spectroheliographs, which provide full-disk solar images in several bands: 175 Å (FeIX–XI, $T_{\max} \sim 1$ MK), 284, 304, and 8.42 Å (MgXII, $T_e \sim 5$–15 MK, $T_{\max} \approx 9$ MK). The SPIRIT has been observing the Sun starting from August 15, 2001 on. In addition to the well-known EUV emission lines, the 8.42 Å line images represent new type of observations of hot coronal plasma, which have not yet been comprehensively investigated.

The SPIRIT sometimes observes in the high-temperature MgXII 8.42 Å line rather large features (with

a size of up to 300 Mm), which exist for many hours high in the corona (Zhitnik et al. 2003). Those features look like a "ball" or "spider" with legs directed downwards. Possible candidates to be identified with those features are post-eruptive arcades, well-known solar features observed many times before, e.g., with *Yohkoh*/SXT. We note in this connection the difference between the SPIRIT MgXII 8.42 Å channel and the SXT (Tsuneta et al. 1991). The temperature sensitivity range of the SXT was rather wide, roughly 2.5–25 MK. Therefore, this telescope showed overlapping different-temperature structures with no reference to a particular temperature. Using the filter ratio method (Hara et al. 1992), it is possible to compute temperature and column emission measure maps from *Yohkoh*/SXT images under some assumptions. By contrast, the SPIRIT MgXII 8.42 Å data supply monochromatic images, whose temperature sensitivity range is narrower (5–15 MK), and this range is centered on a higher temperature of about 9 MK.

Formation of post-eruptive arcades often proceeds energetically, in a form of a post-eruptive flare with predominant emission of accelerated electrons, related to more or less strong magnetic fields rather low in the corona (cf. Švestka 2001). Later on, plasmas confined in the arcade undergo thermalization, and thermal emission of plasmas is assumed to predominate. Analyses of post-eruptive arcades observed in various spectral domains have been addressed in several papers (e.g., Ichimoto et al. 1993, Harra-Murnion et al. 1998, Altyntsev et al. 1999, Grechnev et al. 2004). There are two circumstances in this connection, which have not yet been completely understood.

First, as Borovik et al. (1989) stated, the time scale of an off-limb post-flare coronal source observed in microwaves and millimeters, several hours, strongly suggests excessive energy supply during the post-flare stage. McTiernan et al. (1993) reported that the cooling time observed for hot post-eruptive (post-flare) loops to be too long for the conductive cooling (which is known to work effectively at high temperatures), and that the cooling rate is consistent with the radiative way. They concluded that either thermal conductivity is suppressed, or a long-term heating takes place. Harra-Murnion et al. (1998) also stated that the cooling times deduced from observations of two other events are longer than the theoretically expected ones, and the discrepancy increases with time. Getman & Livshits (2000) and Livshits et al. (2002) modeled behavior of hot plasmas in giant post-flare loops and concluded again that a long-term heating is necessary to provide their properties observed. In principle, the observed properties are explainable in terms of the "CSHKP" ("standard") flare model (Carmichael 1964, Sturrock 1966, Hirayama 1974, Kopp & Pneuman 1976) with magnetic reconnection above the loops. However, the heating rate in the post-flare reconnection site would remain in this case sufficiently high and long-lasting to keep the observed plasma temperature and density.

Second, as Ichimoto et al. (1993) reported, estimates of the relation between the gas and magnetic pressure in an arcade observed after the X9 flare of November 2, 1992, resulted in unexpectedly high plasma beta $\beta = P_{\rm gas}/P_{\rm mag} = 2nkT/(B^2/8\pi) \simeq 1$. Altyntsev et al. (1999) in their multi-spectral study of this event attracted microwave data and concluded that, under the usual assumption of optically thin microwave free-free emission from the arcade, the magnetic field strength inferred from the microwave polarization data can be sufficient to balance the plasma pressure. However, as Grechnev et al. (2004) showed, even a small non-thermal gyrosynchrotron emission can contribute the whole polarization observed in a post-eruptive arcade. Shibasaki (1999, 2001) proposed that high-beta conditions are possible for unstable features in the solar corona, and Getman & Livshits (2000) showed that this is also possible for rather stable features. Gary (2000) showed that the transition from $\beta < 1$ to $\beta > 1$ in the corona occurs at some hundreds km above non-flaring active regions.

On the other hand, observations of long-living radio sources (some of them being off-limb at a height up to 170 Mm) in microwaves and millimeter waves have been reported in several papers (e.g., Urpo et al. 1989, Borovik et al. 1989). These sources were related with post-flare manifestations, but, because no regular soft X-ray observations were available at that time, they could not be directly identified with post-eruptive arcades. Also, it was not possible to separate in those studies the temperature and emission measure contributions. Therefore, Urpo et al. (1989) considered the possibilities of optically thin emission from hot plasmas with $T_e = (5-10)$ MK, which resulted in $N_e = (8-11)\cdot 10^9$ cm^{-3}, and optically thick emission from cold plasmas with $T_e \approx 10^4$ K. As can be easily seen, assuming the former possibility, one obtains $\beta \sim 1$ with $B \sim 20$ G.

Borovik et al. (1989) studied such an off-limb feature and found the microwave polarization to be very high, corresponding for thermal bremsstrahlung to the magnetic field strength of about 300 G at a height of 50–100 Mm. Such strong magnetic fields seem unlikely at that height (cf. Dulk and McLean, 1978); however, no convincing confirmation or denial was found. Also, no direct magnetic field measurements in the corona have been available up to the recent time.

It is well established that hot plasma in post-flare loops is evaporated from the chromosphere. Therefore, the measured high plasma beta corresponds mostly to the evaporated plasmas. We know only few papers where the reconnection rate and parameters of evaporated plasmas have been addressed in a self-consistent way by the numerical solution of MHD equations. Yokoyama & Shibata investigated a simplified model of a two-ribbon flare and its outcomes in a series of papers (e.g., of 1998, 1999, 2001). They showed evaporated plasma beta to be rather high, even close to unity under typical coronal conditions. However, they intuitively restricted its possible maximum value by about unity. They applied the model to the impulsive phase and the early decay of a flare. On the other hand, the observations mentioned above and ours suggest that the standard flare model elaborated by Shibata

& Yokoyama describes quantitatively parameters of post-flare loops even many hours after the impulsive flare energy release.

So, both these issues, the long-lasting heating and high plasma beta at large heights in the corona may have explanation in terms of the "standard" flare model. Note that not all solar astronomers believe in applicability of this model for the initial, impulsive stage of a solar flare.

In this paper, we first identify the large-scale hot feature observed with the CORONAS-F/SPIRIT in the MgXII line. We are interested in plasma parameters in those long-living high-temperature features, because even simple estimations really show that plasma beta in them might not be small. This follows just from the fact that the feature was bright, and it was observed at 100 Mm in the emission line with a maximum at 9 MK. Thus, plasma beta should be carefully addressed.

We can estimate plasma parameters in that feature from soft X-ray *Yohkoh*/SXT data, because observations with SPIRIT were limited on that day, and its spectra are not available for this observation. Using microwave observations with the Nobeyama Radioheliograph (NoRH, Nakajima et al. 1994) at 17 GHz, the Siberian Solar Radio Telescope (SSRT, Smolkov et al. 1986; Grechnev et al. 2003) at 5.7 GHz, and multi-frequency one-dimensional observations from 2.8 to 15.6 GHz with the solar facility at the RATAN-600 radio telescope (Bogod et al. 1993), we can reveal coronal magnetic fields by means of radio astronomy methods. We can also compare them with extrapolations of the photospheric magnetic fields (Rudenko 2001).

Our approach is as follows. In studying solar phenomena, comprehensive data sets in various emissions put different observational constraints on physical conditions and scenarios considered. Analyzing them, one loses freedom to speculate, but gains confidence that the estimates obtained from various observations using different methods are reliable, the interpretation is robust, and this everything is consistent with different observational facts.

For the initial analysis of data from the CORONAS-F soft X-ray and EUV telescopes, which operate since August 2001, it is reasonable to choose a post-eruptive arcade observed simultaneously with the soft X-ray telescope (SXT) on *Yohkoh* (operated by December 14, 2001), which had a relatively close temperature sensitivity range, and whose characteristics are well studied. This reason has determined the choice of a feature observed on October 22, 2001 (this observation and the results of its analysis were briefly reported by Borovik et al., 2005). The present paper contains the first detailed analysis of such a kind of SPIRIT observations (first briefly reported by Zhitnik et al., 2003) using additional data acquired in several spectral ranges. We present SPIRIT images, estimate plasma parameters from soft X-ray *Yohkoh*/SXT data and from microwave observations with NoRH, RATAN-600, and SSRT, as well as EUV SOHO/EIT data. We confirm the results by the agreement of estimates obtained using different observations and methods, and then discuss their physical implications. We show that the SPIRIT MgXII 8.42 Å observations provide pointing at features that are of special interest for the solar plasma physics. Section 2 of this paper describes observations with the SPIRIT and various other instruments in different spectral domains. Section 3 is devoted to estimations and simulations made from the observational data. Section 4 discusses the results, and the conclusions are summarized in Section 5.

2. Observations

A large-scale hot feature of our interest was observed above the SW limb with the CORONAS-F/SPIRIT complex at 10:13–10:22 (times hereafter are UT) on October 22, 2001 (observations in the SPIRIT MgXII 8.42 Å channel were limited on that day). In 8.42 Å images it "looks like a ball" (Fig. 1h, Fig. 2b). The height of its brightest part is about 115 Mm. Images obtained with other instruments within the same field of view in soft X-ray, EUV, and microwave emissions show an arcade.

2.1. Identification

Different instruments show in Figure 1 the pictures corresponding to different temperature ranges. The hot MgXII feature is spatially close to the arcade observed in soft X-rays with *Yohkoh*/SXT or coincides with it. The arcade observed in cooler coronal EUV lines adjoins to the hot MgXII feature and the arcade in *Yohkoh*/SXT images from below. The arcade was observed in the 304 Å SPIRIT channel (Fig. 1a) likely due to hotter coronal lines, which contribute to this passband. Dissimilar appearance of the arcade in different emissions is due to 1) different temperature ranges; 2) different instrumental characteristics, in particular, the spatial resolution; 3) different observation times. Taking into account all these facts, we conclude that the hot feature observed with the CORONAS-F/SPIRIT in MgXII 8.42 Å channel on October 22, 2001 is really associated with hot loops in the top part of an arcade.

The full-disk *Yohkoh*/SXT movie shows that the hot arcade existed many hours before and after the CORONAS-F/SPIRIT observations. It probably formed in the course of eruptive events that occurred on that day. SOHO/LASCO recorded three CMEs on October 22 at the position angles approximately corresponding to the position of the arcade, i.e., at 00:50 (the position angle of 260°), at 03:26 (258°), and at 09:26 (252°). The ejection at 00:50 likely occurred in the active region 9658 near or behind the western limb and was accompanied by a subflare of SF/M1.0 importance. The full-disk *Yohkoh*/SXT movie shows appearance of a large bright loop southward of the hot feature observed with the CORONAS-F/SPIRIT at about 02:40, and at about 05:30 the arcade takes shape similar to that observed around 09 UT. However, we note that there are no full-disk *Yohkoh*/SXT images in the intervals of 01:00–02:40 and 02:50–05:30. Hence, we cannot judge unambiguously with which particular CME the appearance of the arcade was associated. All of them correspond to its position angle, and

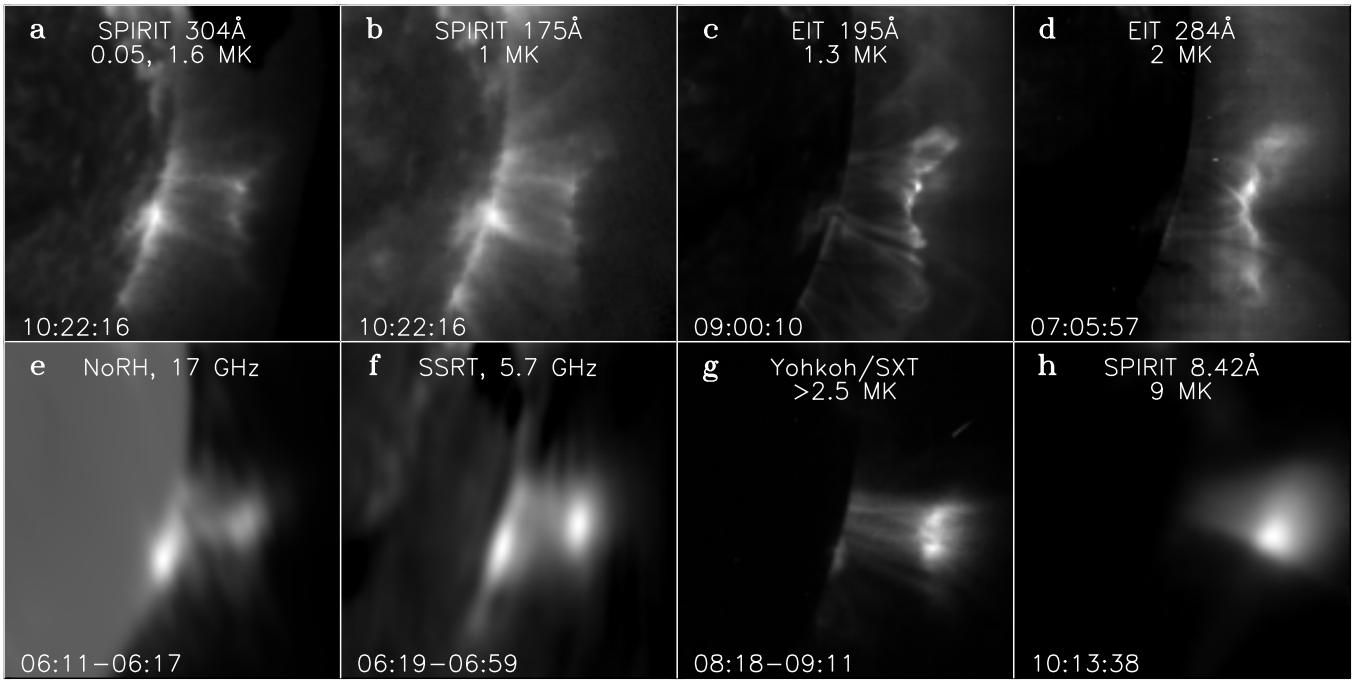

Fig. 1. The post-eruptive arcade observed on October 22, 2001 in various emissions. EUV: SPIRIT at 304 Å (a) and 175 Å (b); EIT at 195 Å (c) and 284 Å (d). Microwaves: NoRH at 17 GHz (e) and SSRT at 5.7 GHz (f). Soft X-rays: *Yohkoh*/SXT (g) and SPIRIT at 8.42 Å (h). All images are shown hereafter non-linearly to emphasize features under consideration.

Yohkoh/SXT images do not provide decisive information.

2.2. Relative Position of the Arcade Observed in Different Emissions

Figure 2[1] shows the relative position of the arcade as observed with different instruments in various emissions. In both panels, grayscale background shows a SOHO/EIT 195 Å image, and white contours show the arcade observed with *Yohkoh*/SXT. Top panel (a) also shows the NoRH image observed at 17 GHz as a light-gray contour (level of 10 000 K). Bottom panel (b) also shows dark-gray contours of the CORONAS-F/SPIRIT image in the MgXII line. The coalignment accuracy of the MgXII image is not perfect, but uncertainties do not allow to shift it sunward. So, the hot MgXII feature is either spatially close to the arcade observed in soft X-rays with *Yohkoh*/SXT, or somewhat higher. The arcade observed in cooler coronal EUV lines closely adjoins to the hot MgXII feature and the arcade in *Yohkoh*/SXT images from below. Moreover, the different-temperature soft X-ray and EUV images even interlace with each other beneath the hot arcade. This shows again that temperature gradients are high, and the temperature increases with height in the arcade region, which was noticed not once before (cf. Ichimoto et al. 1993, Harra-Murnion et al, 1998).

2.3. Microwave Observations

The NoRH shows the arcade at 17 GHz, and the SSRT shows it at 5.7 GHz (Fig. 1e,f). The RATAN-600 one-dimensional Stokes I and V scans at the highest frequency available of 15.6 GHz are shown in Figure 3 along with SPIRIT data observed at 175 Å and 8.42 Å.

2.3.1. Observations with RATAN-600

The RATAN-600 high-sensitivity one-dimensional scans show a weak off-limb source which looks like a small shoulder approximately cospatial with the arcade. This relation persists at many frequencies from 2.8 to 15.6 GHz around 09 UT (Fig. 3, bottom). There were no observations at higher frequencies on that day.

The RATAN-600 data have two major advantages of very high sensitivity due to the huge effective area of the antenna system, and multi-frequency observations in a wide range from 1.0 to 17 GHz. However, there are two disadvantages, the ambiguity of the one-dimensional data and instrumental contributions that are maximal at the solar limb. The instrumental polarization due to specific antenna configuration as the by-limb enhancement is well visible in Stokes V scan shown in Fig. 3b. This instrumental contribution can be eliminated using observations on other days, when neither by-limb, nor off-limb sources were present. In addition, the quiet Sun's envelope makes difficult extraction of the total intensity source in many cases. However, for the observations on October 22, 2001, this problem is not crucial, because on two next days, October 23 and 24, there were no active regions close to the western solar limb, and we referred to those observations. This allowed us to separate reliably both the limb and off-limb sources in the high-frequency part of the operating range both in the total intensity and the

[1] Color version of this figure was presented by Borovik et al. (2005)

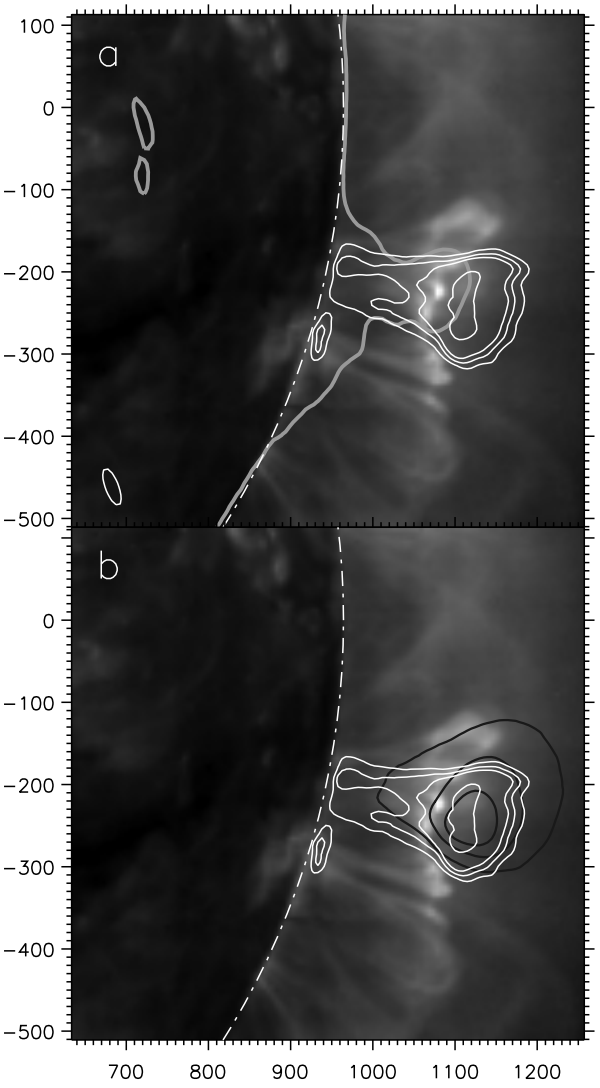

Fig. 2. The overlay of various images of the arcade. Background: SOHO/EIT 195 Å, white contours: *Yohkoh*/SXT. Light-gray contour (a): NoRH, Stokes I at 17 GHz (10^4 K), dark-gray contours (b): SPIRIT 8.42 Å. Small ellipse in the lower left corner in panel (a) shows the NoRH beam. Axes show arc seconds from the solar disk center.

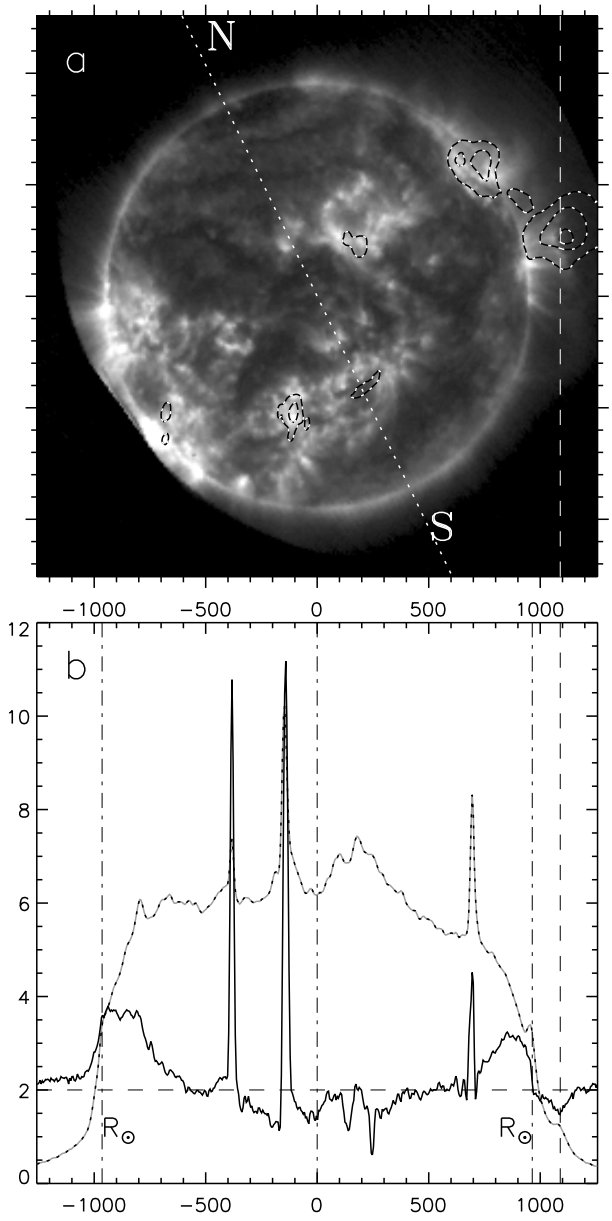

Fig. 3. Observations with SPIRIT and RATAN-600. Top: SPIRIT 175 Å image (halftone) overlaid with contours of the image in MgXII line. The images are rotated to fit the orientation observed by RATAN-600, and the dotted line shows the polar axis of the Sun. Bottom: raw RATAN-600 scans at 15.6 GHz, Stokes V (solid) and Stokes I (gray dotted). Dashed line marks in both panels the polarized off-limb source observed with RATAN-600. Dash-dotted lines mark the photospheric limb and the solar disk center.

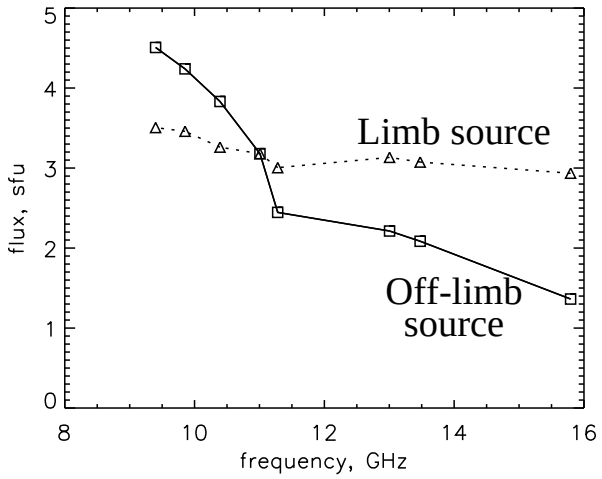

Fig. 4. Microwave spectrum of the arcade according to RATAN-600, solid: off-limb source, dotted: limb source.

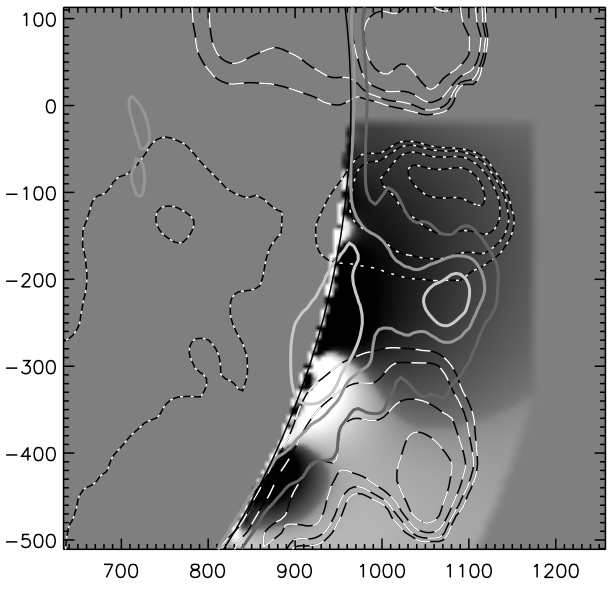

Fig. 5. Contours: microwave polarization of the arcade environment observed with NoRH in the interval 06:11–06:17 (dashed positive, dotted negative, levels of $\pm[0.5, 1, 2, 4]\%$). Halftone background shows coronal magnetic fields (line-of-sight component) extrapolated in the potential approximation. Solid contours show the total intensity observed with NoRH ([5, 10, 15] thousand K).

polarization.

The microwave spectrum measured from the RATAN-600 data is shown in Figure 4. The error in flux measurements of ± 0.3 sfu is determined by the accuracy of both the separation of a source and the calibration technique. The total flux of the off-limb source data grows with a wavelength from 1.3 sfu at 1.9 cm to 4.5 sfu at 3.2 cm, whereas the spectrum of the limb source is practically flat, about 3 sfu in this range. It is difficult to separate the off-limb and limb sources correctly at longer waves due to insufficient spatial resolution of the telescope. The trough at 11.3 GHz ($\lambda = 2.67$ cm) visible at the both curves is obviously also due to instrumental problems.

The limb source (likely due to emission of low coronal loops above the trailing part of AR 9658) steadily existed before and after the eruptions for at least some hours. Hence, it was not related to the eruptive activity. We are not interested in the limb source itself, we only use it as a convenient reference source with its purely thermal, flat microwave spectrum in our study of the microwave spectrum of the off-limb source.

The off-limb source in RATAN scans is distinctly polarized, which promises the possibility to reveal the large-scale magnetic configuration in the corona. This encouraged us to try also to reveal the polarization in two-dimensional NoRH data (it is not detectable in standard snapshot-mode images (integration time of 1 s).

2.3.2. Observations with NoRH

To detect very weak polarization in NoRH images, we produced them with a non-standard, very long integration time of 120 s. Furthermore, we have averaged 4 images in the interval of 06:11–06:17 and 7 images in the interval of 06:15–06:27. The fluctuation sensitivity in those images is enhanced up to at least ~ 20 K. Using those high-sensitivity NoRH images, we have computed the degree of polarization, suppressing unreliable regions in the same way as described by Grechnev et al. (2003). In the computation, all pixels, corresponding to those in both Stokes I and V maps with values below the sensitivity level (we specified $\simeq 40$ K) or below the dynamic range (-25 dB in this case) with respect to the brightest source in the whole full-disk image, were zeroed everywhere in the map. In addition, the result was subjected to the two-dimensional median filtering to suppress possible local defects less than the beam size.

The results are shown in Figures 5 and 6. The degree of polarization shows a relatively short-term appearance of a positively polarized region southward of the arcade (Fig. 5), whereas the dominant negative polarization northward of the arcade (Stokes $V \simeq 60$ K, Stokes $I \simeq 1000$ K for the patch of maximum polarization) persists during the whole imaging interval (Fig. 6). The polarization within the arcade is close to zero.

Figure 6 also shows a RATAN-600 Stokes V scan (the central time is 08:58:07) along with the one-dimensional scan computed from the two-dimensional NoRH Stokes V map, properly oriented and "de-rotated" to the observation time at the RATAN-600. The RATAN-600 scan is processed to suppress instrumental effects. Its by-limb part containing large instrumental contribution is not plotted. The polarized off-limb diffuse source coincides in both scans, with the polarized on-disk compact source also being cospatial. The position angle of 25.7° corresponds to observations at the RATAN-600.

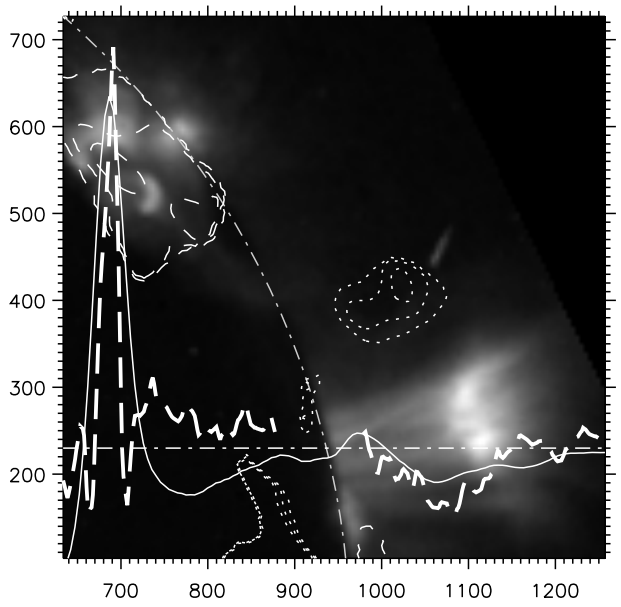

Fig. 6. Hot part of the arcade observed with *Yohkoh*/SXT (background) with overlaid microwave polarization. Closed contours show the degree of polarization observed at 17 GHz in the interval 06:15–06:27, dashed positive ([0.2,2,10]%), dotted negative (−[5, 7.5, 10]%). Thin solid line represents the Stokes V scan computed from NoRH image. Thick broken line represents the Stokes V scan observed with RATAN-600 at 15.6 GHz. The orientation is changed to fit RATAN observations.

2.3.3. Observations with SSRT

Fig. 1f shows an SSRT image of the arcade in total intensity averaged in the interval of 06:19–06:59. The 5.7 GHz images are rather similar to those observed with the NoRH at 17 GHz. The brightness temperature of the by-limb source at 5.7 GHz is ≈ 10 times higher than at 17 GHz ($T_{B\,17} \leq 30\,000$ K), which suggests optically thin free-free emission, but the arcade top in the SSRT image is about 1.5 times brighter then one would expect from the squared frequency ratio. There is no detectable polarization in SSRT data, whose sensitivity seems to be insufficient.

2.4. Dark Features Moving Downward observed in soft X-rays

A movie composed from several *Yohkoh*/SXT images shows dark features moving onto the arcade from above. It is rather difficult to show this phenomenon in a simple static picture. Therefore, to reveal it, we produced difference frames by subtraction of two first frames (separately for each filter, 08:18:09 for AlMg and 08:18:29 for Al12) from each current frame. Figure 7 shows four of those frames representing dark features moving downward, and the most pronounced of them are labeled 1 and 2. Those features likely represent the same phenomenon as that one addressed by McKenzie and Hudson (1999), McKenzie (2000), Gallagher et al. (2002), Innes et al. (2003), Sheeley et al. (2004), and Asai et al. (2004).

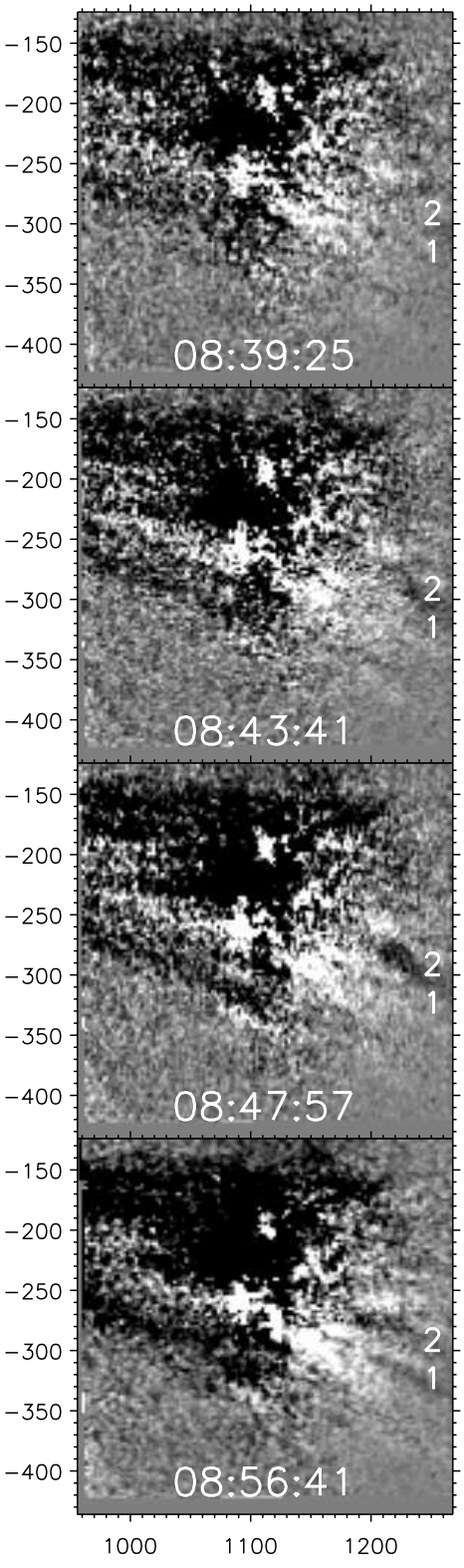

Fig. 7. Difference SXT frames show dark features moving downward onto the arcade. Two of them are labeled 1 and 2. The brightness is limited from both sides to emphasize the dark features.

3. Estimations and Simulations

3.1. Temperature and Density

Using soft X-ray *Yohkoh*/SXT data, we have estimated the temperature and emission measure in the arcade under the assumption of thermal equilibrium using the filter ratio method (Hara et al., 1992; we used the AlMg and Al12 filters) eight hours after the first eruption following known recommendations (e.g., Doschek 1999). We used standard *Yohkoh* software programs SXT_PREP, SXT_INTERP, and SXT_TEEM. The temperature distribution over the arcade region is shown in Fig. 8a. The line filling shows the regions where the estimates are not reliable (we apply the tighter uncertainty level of 0.3 instead of 0.7 used by default). The temperature of the main part of the arcade including its brightest portion is 6 MK, and its upper part has a temperature of up to 8 MK. Column emission measure within a $2.46'' \times 2.46''$ region is $2.5 \cdot 10^{45}\,\mathrm{cm}^{-3}$ for the brightest part. For the resolved loop legs going down, it is about $5 \cdot 10^{44}\,\mathrm{cm}^{-3}$ with a minimum value of $2.5 \cdot 10^{44}\,\mathrm{cm}^{-3}$. To estimate the plasma density, one has to overcome the ambiguity of the depth. To do it, one usually assumes that either the emitting volume is equal to the visible area in the power of 3/2, or that the depth is equal to the width of the emitting area. This way leads us to the estimate of the number density within the brightest part of the arcade of $5 \cdot 10^{9}\,\mathrm{cm}^{-3}$. However, the high brightness of the central portion of the arcade can be also due to an optical (projection) effect. It is possible that the brightness of the loops is uniform at different height, but when they are directed nearly along the line of sight, the column emission measure of the loop tops increases due to the integration. Under such conditions, we should estimate the density using the descending loop leg, and the depth of the emitting volume in this case is equal to the width of the leg. Such an estimate results in $9 \cdot 10^{9}\,\mathrm{cm}^{-3}$. Both estimates are reasonably close, but the second way seems to be more realistic.

With the estimated width of the loop leg and temperature, we estimate the temperature gradient across the descending loop legs. From Figures 1 and 2 (and still better from figure in Borovik et al., 2005) one can conclude that the hot 6 MK plasma in the leg visible in soft X-rays is interlaced with cooler 1–3 MK plasma in the leg visible in EUV at 195 Å. From this fact, we estimate the temperature gradients across the legs of the arcade loops of order $1\,\mathrm{K\,m}^{-1}$. The closeness of the bright arcade top visible in soft X-rays to the "spine" of the EUV arcade also leads to high temperature gradients in the top part of the arcade.

Finally, in Fig. 8b we show the temperature distribution over the arcade region according to the calculations from *Yohkoh*/SXT data (top) along with the dark features moving downward (bottom). The upper panel displays the temperature with black corresponding to 5 MK, white corresponding to 8 MK, and the contour levels are [5.5, 6, 6.5, 7, 7.5] MK. The lower panel shows the same contours of the temperature overlaid on top of the background representing the dark features moving downward. The background image is computed as the minimum along each

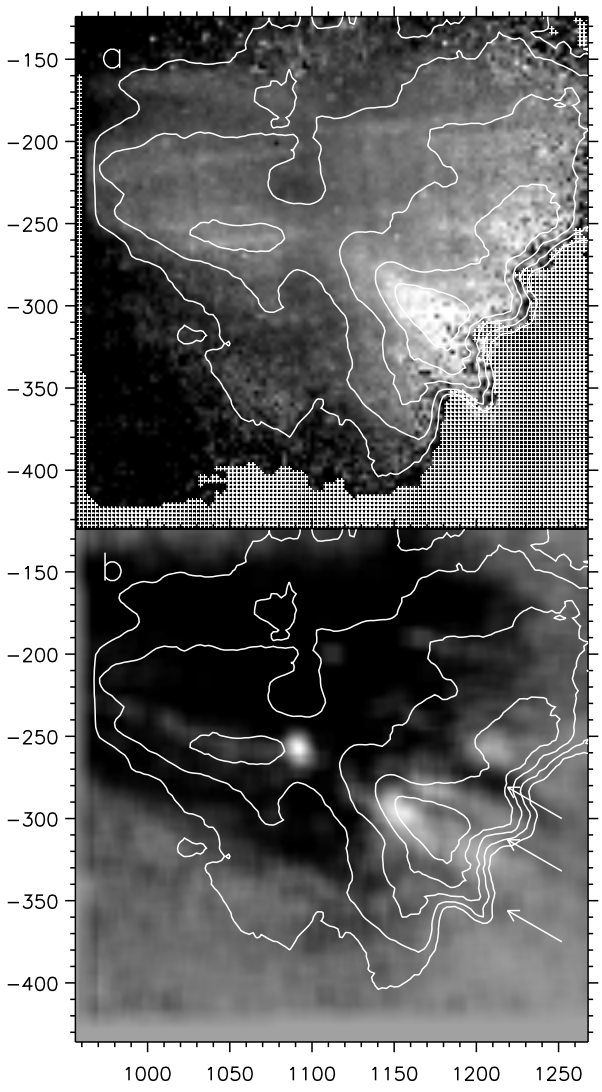

Fig. 8. Temperature distribution over the arcade region according to the calculations from *Yohkoh*/SXT data (top, line filling marks the regions where the estimates are not reliable) along with the dark features moving downward (bottom, three short dark "lanes"). Contours in both panels show the temperature from 5.5 to 7.5 MK. The arrows point out the direction of their motion.

pixel over the difference images from 08:42 to 09:04. Dark moving features show up as three short dark lanes. The arrows point out the direction of their motion. From the figure we see that the temperatures of the regions where they enter the arcade seem to be slightly less than in their vicinity.

3.2. Simulation of Radio Image from Soft X-ray Data

We have computed the optically thin free-free radio emission from soft X-ray data. For this purpose, we used two-dimensional distributions of the column emission measure and electron temperature calculated from *Yohkoh*/SXT full-disk images. For the optically thin limit, $\tau \ll 1$, the brightness temperature $T_{B\nu} \approx T\tau$ with $\tau \approx 0.2 N_e^2 T^{-3/2} \nu^{-2} L$ (e.g., from Dulk 1985). Thus, we obtain $T_{B\nu} \approx 0.2 \cdot EM_{\rm col} T^{-1/2} \nu^{-2} \rho^{-2}$ with $EM_{\rm col}$ being the column emission measure and ρ the pixel size of the image.

Limitations of the dynamic range in measurements of the column emission measure and temperature from *Yohkoh*/SXT data using the filter ratio method put severe restrictions on opportunities of such a simulation due to uncertainties in the measurements of $EM_{\rm col}$ and T_e. The uncertainties become quite large when the signal levels are low. An additional restriction, as Yoshida and Tsuneta (1996) showed, is due to the scattered light in the SXT, which limits the possibilities of correct measurements by 10% of the maximum brightness over a frame. To extend the area of our simulation to fainter regions, we make use of the well-known fact that single-filter *Yohkoh*/SXT images roughly represent the distribution of the emission measure. In this way, we have normalized the thin-filter Al.1 image of 08:56:01 to the obtained brightness temperature distribution using the brightest top part of the arcade. The contribution of uncertainties in the electron temperature must not be high, because the microwave brightness temperature weakly depends on the electron temperature ($T_{B\nu} \propto T^{-1/2}$), and the temperature range of the observed corona is rather limited.

Then we have added the quiet Sun's background, which we found from statistical processing of NoRH images. After that, we convolved the simulated image with the NoRH beam. The result of this simulation shown in Fig. 9b is similar to the observed microwave image at 17 GHz (Fig. 9a). Dissimilarity is due to 1) continuing activity within the two hours (which shows up, in particular, in a little bit larger height of the arcade top in the simulated image), and 2) restrictions of this simulations discussed above. Note again that brighter regions are more reliable.

The brightness temperatures obtained in this simulation are close to the observed values of $(15-25)\cdot 10^3$ K at 17 GHz. This confirms that we really deal with the optically thin case ($\tau_{17} \approx 0.0015 - 0.0025$). This also confirms our estimates of plasma parameters. Moreover, the high temperature within the arcade is confirmed by the SPIRIT observations in MgXII 8.42 Å channel (the temperature sensitivity range 5–15 MK). Note, however, that the arcade top in the SSRT image at 5.7 GHz is about 1.5 times

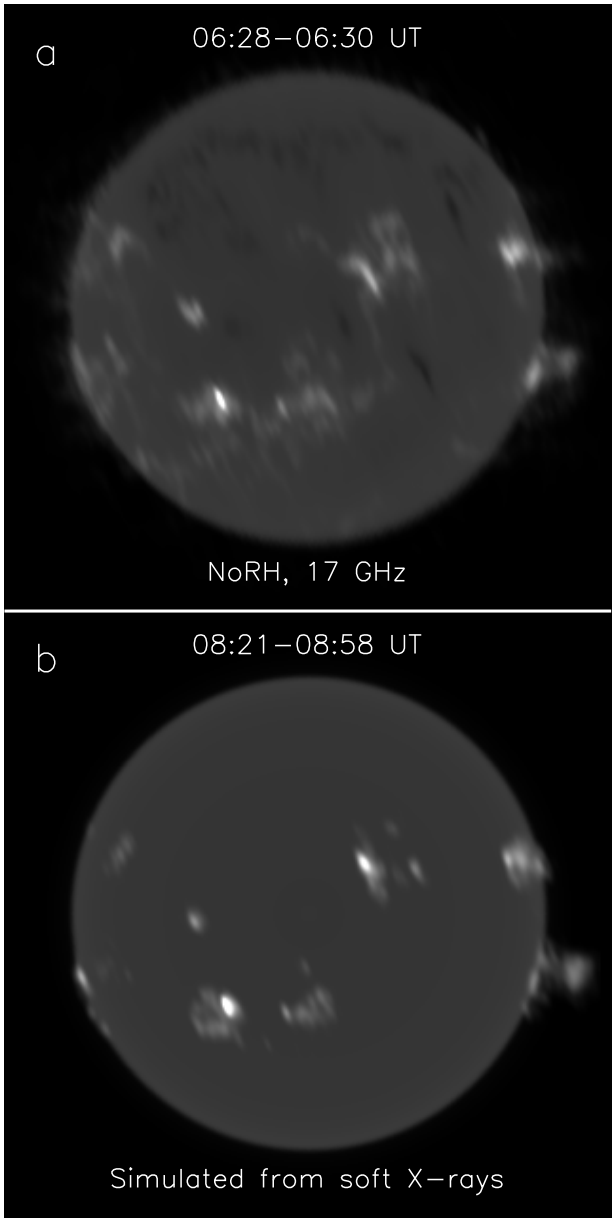

Fig. 9. NoRH image observed at 06:28–06:30 UT (a) and a "radio image" simulated using EM and Te inferred from *Yohkoh*/SXT data two hours later (b). Only sufficiently bright features are reliable.

brighter than it could be expected for the pure case of the optically thin thermal bremsstrahlung (cf. Fig. 1e,f).

The observed brightness temperatures in the Stokes I image within the polarized regions are higher by 500–2500 K than those in the simulated image, while in adjacent non-polarized regions they both do not exceed 800 K, which is likely due to instrumental effects that are present in the NoRH image. These facts support the reality of the polarization shown by the NoRH data.

Similar simulations of microwave images from *Yohkoh*/SXT images data were performed by Grechnev et al. (2003, 2004), but in one-dimensional case and without the absolute calibration. The simulation considered

in this subsection provides independent verification of plasma parameters inferred from soft X-ray data and can be used for the detection of possible gyromagnetic emissions, which visualize coronal magnetic fields and probable presence of non-thermal electrons, and instrumental contributions in the observed microwave images.

3.3. Coronal Magnetic Configuration

To make clearer the situation with the magnetic fields, we consider the photospheric magnetograms. Because the active region of interest was located near the limb, we have to deal with earlier data. Considering SOHO/MDI magnetograms for several days prior to the event along with *Yohkoh*/SXT and SOHO/EIT 284 Å data, we come to the conclusion that the overall large-scale magnetic configuration around the active region persisted almost unchanged for a long time. It was mainly bipolar with the N-polarity at the eastern part and S-polarity at its western part, with a weaker opposite magnetic field in the southeastern part of the large-scale activity complex. The direction of the coronal loops visible in high-temperature emissions above this complex was predominantly latitudinal one, so the configuration observed on the limb corresponds to the previously observed configuration, with the microwave polarization sense corresponding to the x-mode emission.

3.4. Extrapolation of Magnetic Fields into Corona

We have extrapolated the magnetic fields into the corona from the SOHO/MDI photospheric magnetogram of October 19, 2001 in the potential approximation using the method by Rudenko (2001). The line-of-sight component is shown in Fig. 5 along with the degree of polarization map computed from NoRH data averaged within the interval of 06:11–06:17. The overall configuration well corresponds to the polarization observed in microwaves, with the predominant left-handed polarization and a short-term appearance of the right-handed polarization in the region southward of the arcade. The magnitude of the magnetic field extrapolated to a height of 100 Mm is about 7 G. Note that we hardly can expect perfect coincidence of the extrapolated values with the observations, because 1) the magnetogram used for the extrapolation was observed three days before the observations; 2) the results of the potential extrapolation can differ from the reality.

4. Discussion

Soft X-ray *Yohkoh*/SXT and microwave NoRH images show that the formation of the arcade on October 22, 2001 probably started after the first eruption (00:50), and the arcade took shape observed by the CORONAS-F/SPIRIT (10:13) after the second eruption (03:26). Hence, the arcade existed for at least 7 hours keeping its configuration without conspicuous changes. The visible shape of the high-temperature arcade in the CORONAS-F/SPIRIT image is due to the instrumental characteristics of the telescope (in particular, the astigmatism of the optical system). The additional instrumental feature is that the 8.42 Å line is actually a doublet with different focusing, and we see superposition of two slightly displaced images. Furthermore, the wide temperature sensitivity range results in additional smearing out the structures of different temperatures in the images.

Taking into account these instrumental particularities and comparing the relative positions of the images produced with the SPIRIT at 8.42 Å and *Yohkoh*/SXT in Figure 1g,h and Figure 2b (note again that the coalignment accuracy is not perfect) with Figure 8, which shows the temperature distribution obtained from *Yohkoh*/SXT data, one can see that

- both telescopes show the same arcade, although some dissimilarities are present, which can be due to both different instrumental characteristics of the telescopes and different observational times;
- the lower-temperature by-limb loops look fainter in the SPIRIT 8.42 Å image than in the *Yohkoh*/SXT image,
- the highest-temperature part of the arcade in its top with $T_e \geq 7.5$ MK, which is close to the temperature sensitivity maximum of the MgXII 8.42 Å line, roughly coincides with the brightest feature in the SPIRIT 8.42 Å image,
- the upper environment of the arcade disposed to the north and west that is brighter in the SPIRIT 8.42 Å image than in the *Yohkoh*/SXT one suggests its enhanced temperature, which cannot be measured from SXT images using the filter ratio method due to its insufficient brightness.

So, the SPIRIT 8.42 Å images show hot loops in the diverse-temperature arcade structure. This everything is just what can be expected from the difference of the temperature sensitivity ranges of the two instruments and supports both our results and conclusions previously made on the basis of *Yohkoh*/SXT data analyses. In particular, this confirms the fact that the upper parts of arcades have higher temperatures, which was employed many times to support magnetic reconnection high in the corona. This also shows that the combination of data from the SXT and SPIRIT enhances the reliability of information about coronal structures.

Now we shall discuss further consequences, which follow from the analysis of the multi-spectral observations that we have presented.

4.1. Microwave Polarization

Because the microwave polarization computed from the NoRH data is very faint, well below the instrumental limitations of the ordinary NoRH imaging mode, the instrumental polarization clearly shows up in those V maps. Nevertheless, we are confident in the reality of the polarization associated with the arcade region, because 1) the brightness temperatures are rather high in the polarization maps (> 500 K), well exceeding the fluctuation sensitivity level of those images (20 K), 2) its configuration

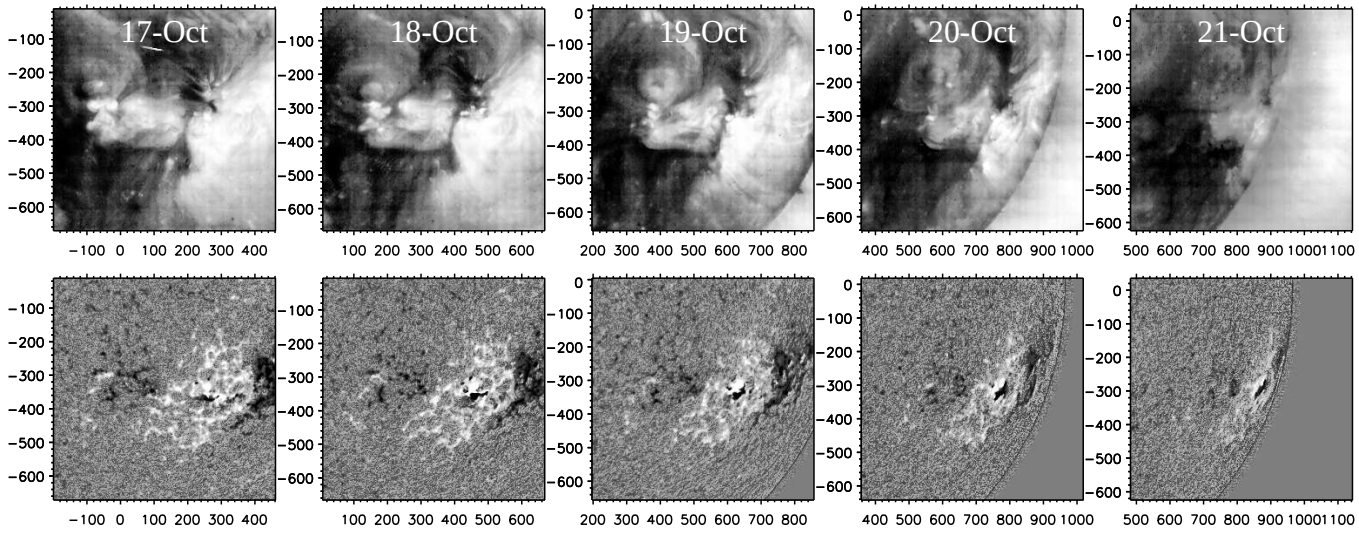

Fig. 10. Coronal configuration observed on previous days with SOHO/EIT at 284 Å near 01:06 UT (upper row) and SOHO/MDI near 01:36 UT (lower row). Axes show arc seconds from the solar disk center. All images are shown non-linearly to emphasize features under consideration.

is significantly different from the instrumental polarization patterns, 3) the polarized region keeps its shape and position in several frames, 4) the polarization in NoRH images is in accord with the polarization measured with the RATAN-600 (Fig. 6), 5) the polarization structure is in accord with the magnetic field configuration extrapolated from a photospheric magnetogram (Fig. 5), 6) the relation of brightness temperatures in the microwave Stokes I image simulated from soft X-ray data and in the really observed one also shows enhancements above the sensitivity level in the polarized regions. All these facts support the reality of the polarization shown by the NoRH data.

It seems for the first glance that the polarization of the microwave emission is due to the optically thin free-free emission in the magnetic field. If it would be really so, than the degree of polarization was determined by the expression $r_c = 2\cos\theta(\nu_B/\nu)$ (Dulk 1985), and from this expression the line-of-sight magnetic field strength $B_\parallel \approx 3\cdot 10^3 r_c$ with r_c being the degree of polarization at 17 GHz. From the NoRH data we obtain that the maximum degree of the negative polarization northward of the arcade is 10 to 12%, which would lead to incomprehensible magnetic fields of ~ 300 G at such a great height. This would strongly contradict the classical estimate by Dulk and McLean (1978), $B \sim 0.5[(R/R_\odot)-1]^{-1.5} \approx 10$ G and disagree with the result of our extrapolation. We note in this connection that recently Lin, Penn, & Tomczyk (2000) and Lin, Kuhn, & Coulter (2004) reported direct measurements of magnetic fields in the corona using Zeeman splitting of the FeXIII 10747 Å line. They found the line-of-sight magnetic field strengths of 10 G at 84 Mm, 33 G at 105 Mm, and 4 G at 72 Mm above three active regions. These results support our assumption that the magnetic field strength of 7 G is much more realistic than 300 G at 100 Mm.

So, we have to recognize that there was a non-thermal contribution: a seemingly negligible addition of 40%-polarized gyrosynchrotron emission with a brightness temperature as few as 250 K could contribute the whole polarization observed. In our case, the microwave spectrum of the off-limb source measured from the RATAN-600 data grows with a wavelength (see Fig. 4). So, the high-frequency part of the off-limb source spectrum rules out its thermal origin. Although we cannot quantitatively estimate the magnetic field strength from the microwave polarization data under the thermal conditions, nevertheless, the polarization does show us the large-scale magnetic configuration high in the corona.

4.2. Magnetic Fields in the Corona

The arcade environment is negatively polarized in NoRH 17 GHz images as well as in RATAN-600 scans at a close frequency of 15.6 GHz, thus delineating the magnetic configuration (x-mode, Fig. 5). The short-term appearance of the positive polarization in NoRH images southward from the arcade shows the presence in that region the large-scale magnetic field of the opposite direction with respect to the region northward from the arcade (N-polarity). The proximity of the opposite large-scale magnetic fields explains the absence of the detectable polarization in the brightest part of the arcade. However, the contour of the negative polarization penetrating the region of the arcade in Fig. 5 shows that the arcade region is polarized in microwaves in the sense of the predominant magnetic field (x-mode). The large-scale coronal configuration is in accord with the observations on the previous days (see Fig. 10), which suggests its relative stability.

As noted in the previous subsection, the magnetic field in the corona is weak at 100 Mm, about 7 G, in accord with our simulation and all above considerations. However, account for the possibility of strong local electric currents and corresponding magnetic fields in compact re-

gions could drastically increase our estimate. There are, however, some circumstances, which rule out such a possibility in our case.

First, the gyrosynchrotron emissivity is known to depend strongly on the magnetic field strength (see, e.g., Dulk 1985). Thus, the presence of strong magnetic field even in a compact region would definitely result in high-intensity gyrosynchrotron emission, which was not observed. Second, non-stationary effects related to the magnetic fields expectable in the impulsive phase of a flare, would result in observable short-term manifestations, which is incompatible with long-term steady conditions in the post-eruptive arcade. The latter fact is also incompatible with the large excess of the magnetic fields of electric currents above the potential fields. Finally, pinching of electric currents is hardly expectable in the post-eruptive arcade under high-beta conditions (see farther). Thus, one has to recognize that the weak magnetic field of about 7 G corresponds to its possible total value. Strong local electric currents can be important during the impulsive phase in regions of strong magnetic fields, where the major flare energy release is observed, unlike the late post-eruptive situation far from those regions, which we deal with.

4.3. Conditions in the arcade

The cooling of a single loop in the arcade must be first dominated by the conductive way, with the characteristic time scale determined by the expression $\tau_c \sim 3N_e kT\,L/q_c$ with $q_c \sim CT^{5/2}(T/L)$ [erg s^{-1}cm^{-2}] thermal flux per unit square, $C \simeq 10^{-6}$ [erg s^{-1}cm^{-1}K$^{-7/2}$], and L the characteristic length. This results in our case in $\tau_c \sim 3$ hours. Then, when the temperature becomes low enough, the radiative cooling becomes appreciable (cf. Aschwanden & Alexander 2001), whose time scale for optically thin coronal plasma with $T > 0.5$ MK is $\tau_r \sim 3N_e kT/Q$ with $Q = N_e^2 R(T)$, $R(T) \simeq 6\cdot 10^{-20}T^{-1/2}$ [erg s^{-1}cm^{-3}] the radiative cooling function due to bremsstrahlung. So, with the same temperature and electron density the radiative cooling time is also about 3 hours. Magnetic reconnection above the arcade can provide the long-lasting heating and appearance of dense post-eruptive loops.

Although the arcade looked steady for a long time, it definitely was neither static, nor purely thermal. Its dynamic state is revealed not only by its slow ascension and inconsistency of its lifetime with the cooling time of a single loop. The following phenomena also confirm this: 1) the changes of its appearance in the SOHO/EIT 195 Å channel, 2) dark features moving down onto the arcade. In addition, 3) the microwave spectrum of the arcade was definitely non-thermal according to the RATAN-600 and SSRT data, 4) the degree of polarization at 17 GHz is incompatible with the thermal nature of the microwave source, and 5) relatively short-term variations of the polarized radio emission shown by NoRH suggest that some non-thermal processes also went on, although they were very faint.

All these facts favor the "standard flare model" ("CSHKP"), but applied to late post-eruptive stages rather than the impulsive phase.

4.4. Relation of gas and magnetic pressure

The magnetic pressure of 7 G estimated at that height is not sufficient to ensure $\beta \ll 1$ usually assumed: even 20 G results in $\beta = 1$. Two statements about closed structures in the solar corona are habitually accepted: a) the magnetic pressure in coronal structures well exceeds the plasma pressure, or $\beta \ll 1$, and b) the magnetic field strength rapidly falls off with height. The two statements forbid existence of long-living closed giant hot structures high in the corona, which have been, nevertheless, sometimes observed. In particular, such structures are exemplified with the post-eruptive arcades of November 2, 1992 analyzed by Ichimoto et al. (1993) and of October 22, 2001, which we present in this paper. Other facts in evidence of the possibility of $\beta > 1$ in the corona have been considered by Gary (2000).

The arcades rather steadily existed for several hours and gradually expanded. Well-known ascension of arcades is generally explained with successive reconnection and cooling of increasingly higher structures. Even if the gas pressure inside the loop exceeds the magnetic one, it would not result in a dramatic outcome. Moreover, the numerical simulations of the flare loop formation performed by Shibata and Yokoyama (1998, 1999, 2001; see Introduction) suggest a simple scaling law for the maximum plasma β in the top part of arcade: $\beta = P_{\rm gas}/P_{\rm mag} = 2N_e kT/(B^2/8\pi) \simeq 0.3(50{\rm G}/B)^2(10^9{\rm cm}/L)(T/10^7{\rm K})^3$. Here L is the characteristic length of the (reconnected) magnetic loop (about the loop height), N_e the number density of the evaporated flare plasma in the loop, B the coronal magnetic field strength, T a temperature in the top of a post-flare loop. This relation can be obtained from expressions (2) and (7) in the paper of Shibata and Yokoyama (1999) by excluding the quiet coronal number density, which is not known in our particular case. Substituting the obtained parameters of $T = 6$ MK, $B = 7$ G, and $L \simeq 10^{10}$ cm into the right-hand part of this expression, we obtain $\beta \simeq 1$. This value is less than the directly measured, $\beta \simeq 4-8$ for the plasma density of $(5-10)\cdot 10^9$ cm^{-3}. The estimates of the plasma β from our observations and from the scaling law by Shibata & Yokoyama both converge to $\beta \geq 1$, although the measured value is larger.[2]

The estimated plasma beta is maximal in a loop filled in with hot evaporated plasma. Later on, it only decreases because of cessation of energy supply into the loop. This leads to decrease of the loop diameter d while the cross-sectional magnetic flux is conserved. Under the assumption that the sum of the magnetic and gas pressure is nearly constant outside and inside the post-eruptive arcade (quasi-static equilibrium), $d \propto (1+\beta)^{1/4}$. The decrease of the plasma beta from the observed $\beta \sim 6$ in a hot arcade loop to the possible $\beta \ll 1$ in that loop after its

[2] Note also that Sheeley et al. (2004) implicitly estimated $\beta > 1$ in the region where the downflow was observed in one event (April 21, 2002), but this estimate is masked due to confusion (page 1231).

cooling results in the decrease of the loop diameter by a factor of 1.6. An additional obscuring of high-temperature loops observed with wide-band soft X-ray telescopes is also obviously due to superposition of diverse-temperature optically thin structures along the line of sight. Both these reasons probably have direct relation to the well-known fact that hot loops appear wide and diffuse in soft X-rays, while cooler loops look thin and well-defined in "cooler" EUV and Hα lines (see, e.g., Tousey et al. 1973, Ichimoto et al. 1993).

4.5. Dark Features Moving Downward

The dark features moving downward onto the top of the arcade seem to visualize the magnetic field structure above the arcade. Such features were first observed in soft X-rays (McKenzie and Hudson, 1999). They can be either due to low column emission measure (very low column density), or due to absorption (very low temperature and high column density). Their depth must be significant; otherwise, they would not be visible because of emission of the material from behind them. McKenzie and Hudson proposed their interpretation as collapsing voids (the former one). Another possibility is that they represent remnants of material of an eruptive filament that fall back (Shibasaki 2002). In such a case, they can be very cool, because material of the eruptive filament must not be necessarily heated (e.g., Uralov et al. 2002).

Then such dark features were also found in EUV observations with TRACE (Gallagher et al. 2002) and white-light observations with SOHO/LASCO (Wang et al. 1999). Innes et al. (2003) analyzed observations of such features with SOHO/SUMER in several emission lines sensitive to temperatures from $2 \cdot 10^4$ to 10^7 K and concluded that they most likely represent voids, according to the initial idea of McKenzie and Hudson (1999). Nevertheless, they noticed manifestations of absorption for the leading part for one of such inflows. Sheeley et al. (2004) analyzed some events in which moving downward dark features were observed, and proposed that they represent newly formed empty loops, shrinking down from the reconnection site.

According to our estimates from *Yohkoh*/SXT data, the inflow regions seem to be cooler than their vicinity. Shibasaki (2002) discussed probable contribution of the kinetic energy of falling remnants of an eruptive filament to the heating the arcade. However, it is difficult to apply this idea to our case.

So, the nature of those dark features still remains vague. Previous results suggest their low density, and our results hint their low temperature. They may also participate in mass supply to the arcade, if they are not empty. A possibility may exist to shed additional light on their origin from observations. Namely, if the dark features represent dense shrinking loops, their dynamic plasma pressure must be higher as compared with the neighborhood. Hence, the underlying part of a post-eruptive arcade may have a dip. However, it can be also difficult to detect the dip reliably because of many observational restrictions along with the absence of stationary picture of their inflow onto an arcade.

5. Summary and Concluding Remarks

1. We have presented CORONAS-F/SPIRIT X-ray and EUV observations and carried out the first detailed analysis of a hot, long-living, large-scale coronal feature observed with the SPIRIT in MgXII 8.42 Å line (temperature sensitivity range of 5–20 MK). We have identified this feature with a hot top part of a post-eruptive arcade.
2. Using data acquired in several spectral ranges, we have estimated plasma parameters in the post-eruptive arcade and verified them using independent methods, in particular, simultaneous observations in different spectral domains. In this way, we applied some special techniques:
   - very weak polarization in NoRH images was revealed using imaging with very long integration time of 120 s, thus enhancing the fluctuation sensitivity up to at least ~ 20 K,
   - comparison of a microwave image simulated from the column emission measure and electron temperature distributions inferred from soft X-ray images with the really observed one, which provides verification of the quantities obtained from observations.

   The plasma parameters estimated for the arcade some hours after the eruption are as follows.
   - From *Yohkoh*/SXT data we have obtained the number density of about 10^{10} cm^{-3} and electron temperature of 6 MK. The estimates are verified independently by a) the observation of the arcade with the CORONAS-F/SPIRIT in MgXII 8.42 Å line, and b) both qualitative and quantitative accord of radio images simulated from soft X-ray data with those really observed. These estimates also agree with known results of other studies. Thus, the independent observations with the SPIRIT provide additional support of conclusions made in previous studies.
   - From high-sensitivity NoRH and RATAN-600 polarization data we have revealed the large-scale coronal magnetic configuration surrounding the arcade at a large height. The potential-approximation extrapolation of the photospheric magnetic fields into the corona also consists with the configuration. Hence, it supplies the plausible strength of $\simeq$7 G.
   - The degree of polarization computed from specially processed high-sensitivity NoRH data and confirmed by RATAN-600 observations leads (under the assumption of free-free emission mechanism) to the magnetic field strength of order 300 G. This is quite unlikely as high as 100 Mm in the corona and contradicts the

result of our magnetic field extrapolation. We therefore conclude that a minor contribution of gyrosynchrotron emission emphasizes the microwave polarization, which is in accord with the steep total flux Stokes I spectrum.

The above result shows that non-thermal processes went on during the late decay of the event. They were faint, but sufficient to supply the whole polarization observed in microwaves. This shows that the coronal magnetic field strength can be well overestimated from radio data, if not all important emission mechanisms are revealed. This also points out importance of spectral measurements in microwaves.

3. The observational results indicate prolonged energy release high in the corona manifesting itself in long-lasting heating capable to keep high temperature in the arcade for a long time with pronouncedly higher temperature of its top part, and in detectable signatures of non-thermal processes, both at late post-eruptive stages. These factors favor, for this kind of phenomena, the configuration and scenario of the "standard flare model".
4. Our analysis shows again that plasma beta can be high, $\beta > 1$, in long-living giant hot coronal structures. The CORONAS-F/SPIRIT observations in the hot 8.42 Å line explicitly indicate this. Our estimate of the cross-sectional expansion of a high-beta loop within the framework of the "standard flare model" with the chromospheric evaporation, elaborated by Shibata & Yokoyama, shows that it is not great, with its width being proportional to $\sqrt[4]{1+\beta}$.
5. We have also addressed dark McKenzie–Hudson features moving downward onto the arcade. They represent either falling down remnants of material of a pre-ejected filament, or collapsing empty loops. From *Yohkoh*/SXT data we have found indications of their low temperature. Those features must have either great geometrical depth, if they are empty, or great optical depth, if they are dense.

Thus, our major conclusions indicate that the "standard flare model" applies to the late post-eruptive phase of the event. They also indicate high-beta conditions that are possible in long-living giant hot coronal loops, which were first pointed out by Ichimoto, Sakurai et al. in 1993, but still not attracted the proper attention.

Acknowledgments. We would like to thank unknown referee for important comments and useful suggestions which helped to improve this paper. We thank the instrumental teams of the NoRH, SSRT, RATAN-600 and CORONAS-F, *Yohkoh*, and SOHO missions for the open-data policies. We are grateful to V. Garaimov for his assistance in processing RATAN-600 data. CORONAS-F is a project of international cooperation between Russian and Ukrainian Space Agencies and Academies of Sciences with participation of Poland, Germany, Slovac Republic, France, Great Britain, and the USA. *Yohkoh* is a project of international cooperation between ISAS and NASA. SOHO is a project of international cooperation between ESA and NASA. We also used the CME catalog generated and maintained by NASA and the Catholic University of America in cooperation with the Naval Research Laboratory. This work is supported by the Russian Foundation of Basic Research under grants 03-02-16591, 03-02-17528, 03-02-17357, 05-02-17105, the Russian Federal Ministry of Education and Science under grants NSh 477.2003.2 and OFN 18, the Presidium of RAS, and the program of the Russian Academy of Sciences "The solar activity and physical processes in the Sun-Earth System".

References

Altyntsev A.T., Grechnev V.V., Nakajima H., Fujiki K., Nishio M., Prosovetsky D.V., 1999, A&AS 113, 415.
Asai A., Yokoyama T., Shimojo M., Shibata K. 2004, ApJL 605, 77.
Aschwanden M.J., Alexander D. 2001, Sol. Phys. 204, 91.
Bogod V.M., Vatrushin S.M., Abramov-Maksimov V.E., Tsvetkov S.V., Dikiy V.N. 1993, ASP Conference Series, 46, 306.
Borovik V.N., Gelfreikh G.B., Bogod V.M., Korzhavin A.N., Krüger A. 1989, Sol. Phys. 124, 157.
Borovik V.N., Grechnev V.V., Bugaenko O.I., Bogachev S.A., Grigorieva I.Y., Kuzin S.V., Lesovoi S.V., Livshits M.A., Pertsov A.A., Rudenko G.V., Slemzin V.A., Stepanov A.I., Shibasaki K., Uralov A.M., Zandanov V.G., Zhitnik I.A. 2005, "Coronal and Stellar Mass Ejections", Proc. IAU Symp. 226, 108.
Carmichael H. 1964, Proc. of AAS-NASA Symp. on the Physics of Solar Flares, W. N. Hess, NASA-SP 50, p. 451.
Doschek G.A. 1999, ApJ 527, 426.
Dulk G.A., McLean D.J. 1978, Sol. Phys. 57, 279.
Dulk G.A. 1985, ARA&A 23, 169.
Gallagher P.T., Dennis B.R., Krucker S., Schwartz R.A., Tolbert A.K. 2002, Sol. Phys. 210, 341.
Gary G.A. 2001, Sol. Phys. 203, 71.
Getman K.V., Livshits M.A. 2000, Astron. Rep. 44, 255.
Grechnev V.V., Lesovoi S.V., Smolkov G.Ya., Krissinel B.B., Zandanov V.G., Altyntsev A.T., Kardapolova N.N., Sergeev R.Y., Uralov A.M., Maksimov V.P., Lubyshev B.I. 2003, Sol. Phys. 216, 239.
Grechnev V.V., Zandanov V.G., Uralov A.M., Maksimov V.P., Rudenko G.V., Borovik V.N., Gelfreikh G.B., Grigorieva I.Y., Medar V.G., Korzhavin A.N. 2004, Sol. Phys. 225, 379.
Hara H., Tsuneta S., Lemen J.R., Acton L.W., McTiernan J.M. 1992, PASJ44, L135.
Harra-Murnion L.K., Schmieder B., van Driel-Gesztelyi L., Sato J., Plunkett S.P., Rudawy P., Rompolt B., Akioka M., Sakao T., Ichimoto K. 1998, A&A 337, 911.
Hirayama T. 1974, Sol. Phys. 34, 323.
Ichimoto K., Sakurai T., Flare Telescope, Norikura Teams. 1993, Proc. 2nd Japan-China seminar on Sol. Phys., p. 151.
Innes D.E., McKenzie D.E., Wang T. 2003, Sol. Phys. 217, 247.
Kopp R.A., Pneuman G.W. 1976, Sol. Phys. 50, 85.
Lin H., Penn M.J., Tomczyk S. 2000, ApJL 541, 83.
Lin H., Kuhn J.R., Coulter R. 2004, ApJL 613, 177.
Livshits M.A., Badalyan O.G., Belov A.V. 2002, Astron. Rep., 46(7), 597.
McKenzie D.E., Hudson H.S. 1999, ApJL 519, 93.
McKenzie D.E. 2000, Sol. Phys. 195, 381.

McTiernan J.M., Kane S.R., Loran J.M., Lemen J.R., Acton L.W., Hara H., Tsuneta S., Kosugi T. 1993, ApJL 416, 91.
Nakajima H., Nishio M., Enome S., Shibasaki K., Takano T., Hanaoka Y., Torii C., Sekiguchi H., Bushimata T., Kawashima S., Shinohara N., Irimajiri Y., Koshiishi H., Kosugi T., Shiomi Y., Sawa M., Kai K. 1994, Proc. IEEE 82(5), 705.
Oraevsky V.N., Sobelman I.I. 2002, Astron. Letters 28(6), 401.
Oraevsky V.N., Sobelman I.I., Zitnik I.A., Kuznetsov V.D., Stepanov A.I., Polishuk G.M., Kovilin P.N., Negoda A.A., Dranovsky V.I., Yatskiv Ya.S. 2003, Adv. Space Res. 32, 2567.
Rudenko G.V. 2001, Sol. Phys. 198, 5.
Sheeley N.R., Jr., Warren H.P., Wang Y.-M. 2004, ApJ 616, 1224.
Shibasaki K. 1999, Proc. of *Yohkoh* 8th Anniversary Symp. "Explosive Phenomena in Solar and Space Plasmas". Sgamihara, December 6–8, 1999. Eds. T. Kosugi, T. Watanabe, M. Shimojo. The Institute of Space and Astronautical Science, p. 93.
Shibasaki K. 2001, ApJ 557, 326.
Shibasaki K. 2002, ApJL 567, 85.
Shibata K., Yokoyama T. 1999, ApJ 526, L49.
Smolkov G.Ia., Pistolkors A.A., Treskov T.A., Krissinel B.B., Putilov V.A. 1986, Ap&SS 119, 1.
Sturrock P.A. 1966, Nature 211, 695.
Švestka Z. 2001, Space Sci. Rev. 95, 135.
Tousey R., Bartoe J.D.F., Bohlin J.D., Brueckner G.E., Purcell J.D., Scherrer V.E., Sheeley N.R., Jr., Schumacher R.J., Vanhoosier M.E. 1973, Sol. Phys. 33, 265.
Tsuneta S., Acton L., Bruner M., Lemen J., Brown W., Caravalho R., Catura R., Freeland S., Jurcevich B., Owens J. 1991, Sol. Phys. 136, 37.
Uralov A.M., Lesovoi S.V., Zandanov V.G., Grechnev V.V. 2002, Sol. Phys. 208, 69.
Urpo S., Teräsranta H., Krüger A., Hildebrandt J., Ruždjak V. 1989, Astron. Nachr. 310(6), 423.
Wang Y.-M., Sheeley N.R., Howard R.A., St. Cyr O.C., Simnett G.M. 1999, Geophys. Res. Lett. 26(9), 1203.
Yokoyama T., Shibata K. 1998, ApJL 494, L113.
Yokoyama T., Shibata K. 2001, ApJ 549, 1160.
Yoshida T., Tsuneta S. 1996, ApJ 459, 342.
Zhitnik I.A., Bougaenko O.I., Delaboudiniere J.-P., Ignatiev A.P., Korneev V.V., Krutov V.V., Kuzin S.V., Lisin D.V., Mitrofanov A.V., Oparin S.N., Oraevsky V.N., Pertsov A.A., Slemzin V.A., Sobelman I.I., Stepanov A.I., Schwarz J. In: Solar variability: from core to outer frontiers. The 10th European Solar Physics Meeting. ESA SP-506, Vol. 2. Noordwijk: ESA Publications Division, 2002, p. 915.
Zhitnik I.A., Bugaenko O.I., Ignat'ev A.P., Krutov V.V., Kuzin S.V., Mitrofanov A.V., Oparin S.N., Pertsov A.A., Slemzin V.A., Stepanov A.I., Urnov A.M. 2003, MNRAS 338, 67.